Optical Ray Tracing Simulation by Using Monte Carlo Method for Reflectance-based Photoplethysmography Sensor in Human Skin and Fingertip Model

Muhamad Affiq Bin Misran[1,a], Anubha Bilgaiyan[2], and Reiji Hattori[1,3]

[1]Department of Applied Science for Electronics and Materials, Kyushu University, Japan

[2]Innovation Center for Organic Electronics, Yamagata University, Japan

[3]Global Innovation Center (GIC), Kyushu University, Japan

[a]email: misran.muhamad.458@s.kyushu-u.ac.jp

Abstract. *The pulse oximetry device has been used for decades to monitor human pulse rate and oxygen saturation. There are two types of pulse oximetry which are transmission and reflection based. However, most devices are unsuitable for daily health monitoring due to the bulkiness and inconvenience of long-term monitoring while continuously doing everyday activities. Therefore, developing a wearable device such as a patch would benefit the users. Several factors can be considered for such a system. One of them is the distance between the source and detector since both are the major components of this system. However, there is still a lack of information in this regard. This study used the ray-tracing Monte Carlo method to simulate transmittance and reflectance-based oximetry principles with a 663 nm wavelength as the light source. The results show the ray tracing behavior from the light source to the photodetector in the biological tissue under two different structures mentioned previously. The separation between the light source and the detector should be less than 3 mm for the reflection type. A significant difference was observed for a distance greater than 3 mm compared with the transmission-based, which has a higher photocurrent even at a 7 mm distance. However, this transmission-based device is limited to the placement of the device on the body part. It is due to the thickness, which varies depending on the body parts themselves. Therefore, wearable pulse oximetry devices with the reflectance-based principle are better due to higher signal acquisition than the transmittance-based, especially for the daily health monitoring system. Furthermore, it also can be used throughout any body part. This reflection-based device can fully utilize microfabrication to integrate the light source and photodetector.*

Keywords: PPG sensor, Monte Carlo, tissue optics, pulse oximetry, photoplethysmography

Introduction

The pulse oximeter is a device that uses a non-invasive technique to monitor oxygen saturation in the blood as an initial procedure before further diagnosing can be performed on a patient [1]. Then, the information from the device is used to appraise the numerous medical conditions related to the behavior of the heart and lungs [2]. In general, pulse oximetry operates in two principles, as shown in Figure 1. The principles are reflection-based and transmission-based, which can be easily purchased from the market.

The pulse oximeter devices comprise two major components. Those components are the light source and the photodetector. The emitted light from the light source is propagated in the skin, blood, bone, and other tissues in different conditions, such as absorbed, transmitted, scattered,

and partially reflected. Then, the photodetector is used to sense the reflected light (reflection-based) or different the different intensities (transmission-based), where it generates the electrical signal [3]. This electrical signal consists of two pieces of information: the AC pulsatile and the quasi-static DC components [4]. These components make the photoplethysmography (PPG) signal, as shown in Figure 2. From Figure 2, the significant DC component corresponds to the light diffusion through the tissues, venous blood, static arterial blood, and skin. In contrast, the small AC signal arises from the differences in light absorption in the arterial blood vessels during the systole and diastole pulsation [5]. The signal helps to provide some preliminary information about the user's health condition since the pulsation (blood flow) itself is controlled by neural, cardiac, and respiratory interactions.
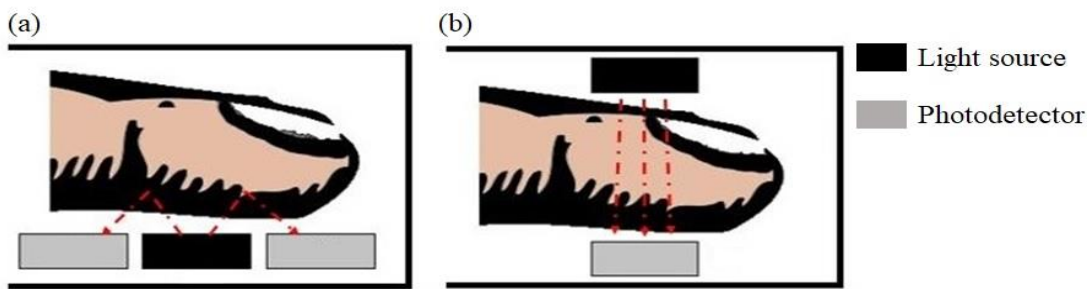
Figure 1. Principle of (a) reflectance-based and (b) transmission-based pulse oximeters.
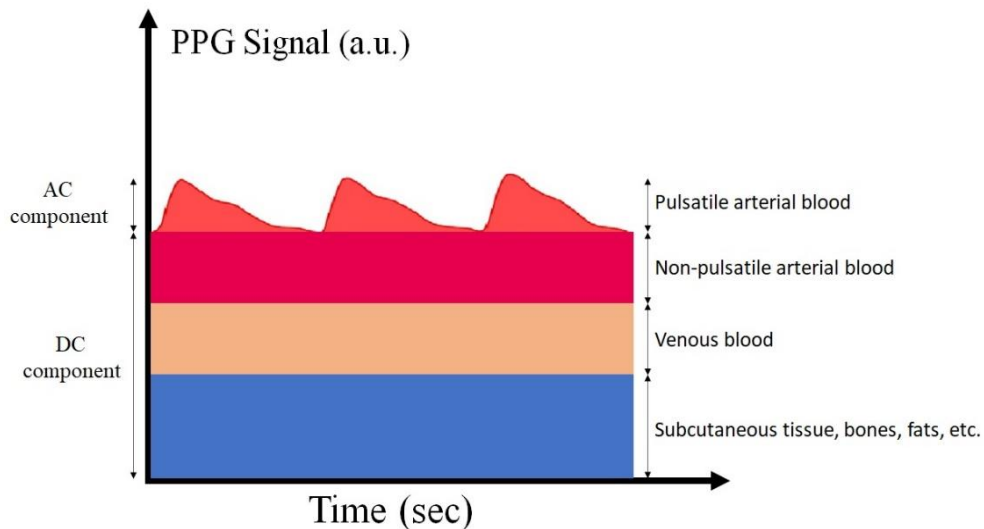
Figure 2. PPG signal components

Several studies have developed the pulse oximeter, especially in recent years, to improve its performance, reliability, and feasibility, mainly as wearable daily health monitoring devices. In

2014, Huang et al. demonstrated the ring-type pulse oximeter with a multi-detector system [6]. In this system, the effect of the light source and detector placement at different angles was investigated and compared with multi-detectors method for measuring arterial oxygen saturation (SpO$_2$). They also indicated that using a multi-detector system can further enhance the PPG signal collection. A higher correlation was observed between their approach and the commercial fingertip-type pulse oximeter. A reflectance-based pulse meter sensor with a circular structure of organic light-emitting diode (OLED) surrounded by the organic photodetector (OPD) at two different distances was fabricated by Elsamnah et al. in 2019 [7]. Their finding shows that a shorter length has a higher signal-to-noise ratio (SNR). Therefore, the light source and photodetector placement can significantly affect the PPG signals. However, there is still a lack of information regarding the optical behavior in the finger structure or turbid media. It is due to the complexity of those structures and the optical characteristics which significantly impact the light scattering behavior in the human body.

The optical human tissue simulation has been widely studied to understand light characteristics and behaviors in the turbid media. This study is crucial to improve the reliability of the devices or applications which use the light source and photodetector as their major components. In 1993, Hiraoka et al. studied the optical path length using the Monte Carlo (MC) method at near-infrared (NIR) in the homogeneous tissue [8]. Reuss et al. also used this MC method in 2004 to investigate arterial pulsation based on the reflectance pulse oximetry on a tissue model [9]. In 2007, Peris et al. established a custom MC method platform, generating the mechanism in pulse oximetry based on the opto-physiological model [10]. Then, Chatterjee et al. also analyzed the optical interactions in reflectance and transmittance finger PPG using the MC method in 2019 [11]. Thus, studying the interaction between light and human skin is necessary to provide reliable and valuable information for further enhancing PPG devices.

In this study, we used the LightTools software with the MC ray tracing method to perform this simulation. A skin model with only a reflectance-based approach was used to observe the ray tracing internally. Then, a fingertip model was used to monitor the ray tracing based on the reflectance and transmittance principles. We tried to imitate the pulsation condition by changing the thickness of the highly oxygenated blood layer for the skin structure and the artery's diameter for the fingertip structure. Then, we estimated the optimum distance between the light source and detector for the pulse oximetry device.

Materials and Methods

The present study used the LightTools software with the MC method for the optical ray tracing for the optical simulation. The geometry and structure of models are discussed here. Other information, such as the optical properties of the materials used in this simulation, also is explained here.

Geometry of the skin and finger structure

The skin tissue model used in this simulation is shown in Figure 3, comprising three main layers. The epidermis is the outer skin layer composed of dead cells as a protective layer. The dermis is a layer that acts as a cushion for the inner layer and consists of the plexus superficials and the plexus profundus layers. Many blood capillaries exist in this layer, especially in the plexus profundus, where the pulsatile condition occurs. The bottom layer is the subcutaneous or

hypodermis layer, mainly composed of fat and other tissues. The construction of the skin model used in this simulation is summarized in Table 1 [9,12-16].
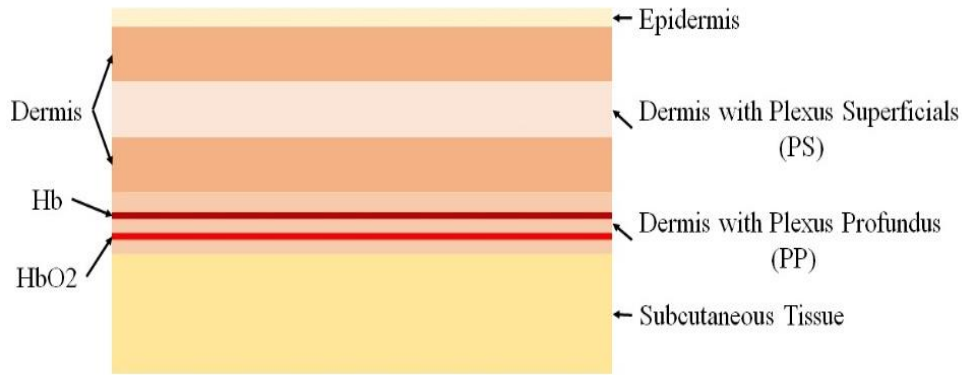

Figure 3. Skin tissue model

Table 1. Human skin model thicknesses

Layer	Sublayer	Thickness (mm)
Epidermis	-	0.2
Dermis	Dermis 1st layer	0.2
	Plexus Superficials	0.2
	Dermis 2nd layer	0.9
	Plexus Profundus	0.6
	Hb	0.06
	HbO_2	0.012 (initial) 0.060 (pulsatile)
Subcutaneous Tissue	-	4.0

The fingertip structure consists of muscles, bone, and tendons, where the size of each of them differs between individuals. Therefore, there is no standard size for this model. The basic fingertip structure was considered for simplicity, as shown in Figure 4, with the dimension used [6,17-19].
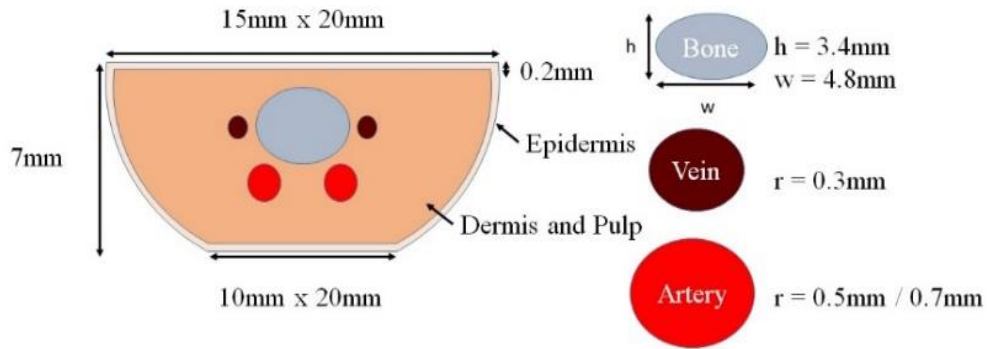
Figure 4. Fingertip structure model

Optical simulation by Monte Carlo (MC) method

The light is treated as a bundle of photons transported in the turbid media in the MC simulation. The trajectories of photons in the media are determined by the random numbers generated by a computer statistically and characterized by several optical parameters. The Henyey-Greenstein distribution is commonly used in biomedical optics, where it is applied in the LightTools software, and the function is given by [20]:

$$p(\theta) \ = \frac{1}{4\pi} \cdot \frac{1-g^2}{(1+g^2-2g.cos(\theta))^{\frac{3}{2}}} \qquad (1)$$

where θ is the scattering angle, and g is the scattering anisotropy parameter. The value of g is represented by the cosine of the scattering angle as given by [20]:

$$g \equiv \langle cos\,\theta \rangle = \int_0^\pi p(\theta)\,cos\,\theta \,.\, 2\pi\,sin\,\theta d\theta. \qquad (2)$$

Several essential parameters for the optical human tissue simulation will determine the behavior of the light scattering and distribution in the human tissue. These optical properties are the refractive index (η), anisotropy parameter (g), absorption coefficient (μ_a), scattering coefficient (μ_s), and Mean Free Path (MFP). These optical parameters are summarized in Tables 2 and 3 [6,9,21,22].

Table 2. Optical properties for the human skin structure.

Material	Refractive Index (η)	Anisotropy parameter (g)	Absorption Coefficient (μ_a) in mm^{-1}	Scattering Coefficient (μ_s) in mm^{-1}	MFP in mm
Epidermis	1.433	0.79	0.27	10.7	0.093458
Dermis	1.396	0.81	0.27	18.7	0.053476
Dermis with	1.396	0.82	0.27	19.2	0.052083

Plexus Superficials Dermis with Plexus Profundus	1.400	0.78	0.27	22.5	0.044444
HbO$_2$	1.363	0.98	0.20	77.5	0.012900
Hb	1.362	0.98	0.72	77.5	0.012800
Subcutaneous Tissue	1.370	0.75	0.003	5.0	0.20000

Table 3. Optical properties for the human fingertip structure.

Material	Refractive Index (η)	Anisotropy parameter (g)	Absorption Coefficient (μ_a) in mm^{-1}	Scattering Coefficient (μ_s) in mm^{-1}	MFP in mm
Epidermis	1.433	0.79	0.27	10.7	0.093458
Dermis and pulp	1.380	0.91	0.05	8.6	0.115600
Bone	1.400	0.92	0.05	33.1	0.030100
HbO$_2$	1.363	0.98	0.20	77.5	0.012900
Hb	1.362	0.98	0.72	77.5	0.012800

Simulation process

This simulation was performed on the fingertip structure based on both principles. However, only reflection-based was applied for the skin structure since the feasibility of the transmission-based pulse oximetry does not apply to the thicker area of human body parts such as the arm and forehead. Figures 5 and 6 show the configuration between the light source and the detector placement used in these simulations.
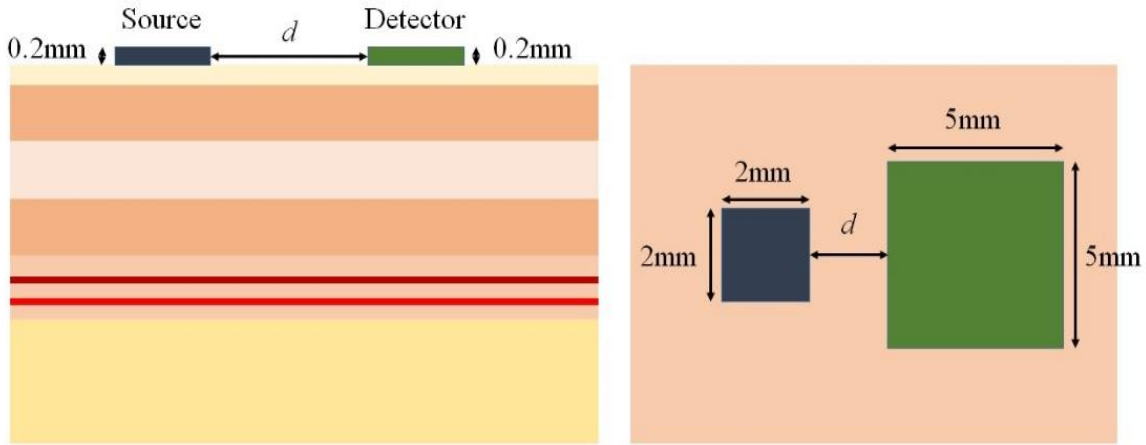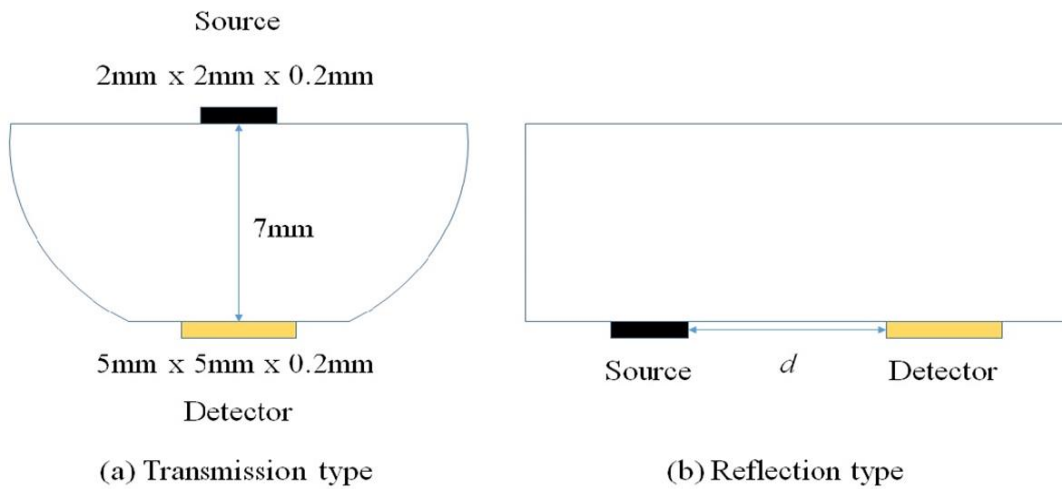
Figure 5.   Fingertip structure model

Figure 6.   Transmission (left) and reflection (right) type of the simulation setup

These simulations used 633 nm (red light) wavelength at 1 mW radiometric power as the light source. It has surface illuminance and the Lambertian characteristics for the light's angular distribution. At the same time, the detector has surface detection to observe and measure the number of photons that arrive at the detector surface. The pulsatile condition was done by changing the structure thickness. The diastolic mode is assumed to be the initial condition, where it represents the DC component in the PPG signal. In systolic mode, the thickness or radius of HbO_2 in both structures was increased based on Table 1 and Fig. 4. The difference is used to represent the AC component of the signal obtained from the simulation.

Results and Discussion

Ray tracing (Skin and fingertip model)

Figure 7 shows the ray-tracing distribution under the scattering events in the skin model for the reflection-based principle. The distance between the light source and the detector was 0 mm, filtered by the light distributed only related to the HbO2 layer to the detector surface. In this simulation, we used 105 numbers of rays for visualization purposes only, as shown in Fig. 7, whereas 108 numbers of rays for the data collection. Most of the rays were scattered within the dermis layer due to a higher scattering coefficient than other components.
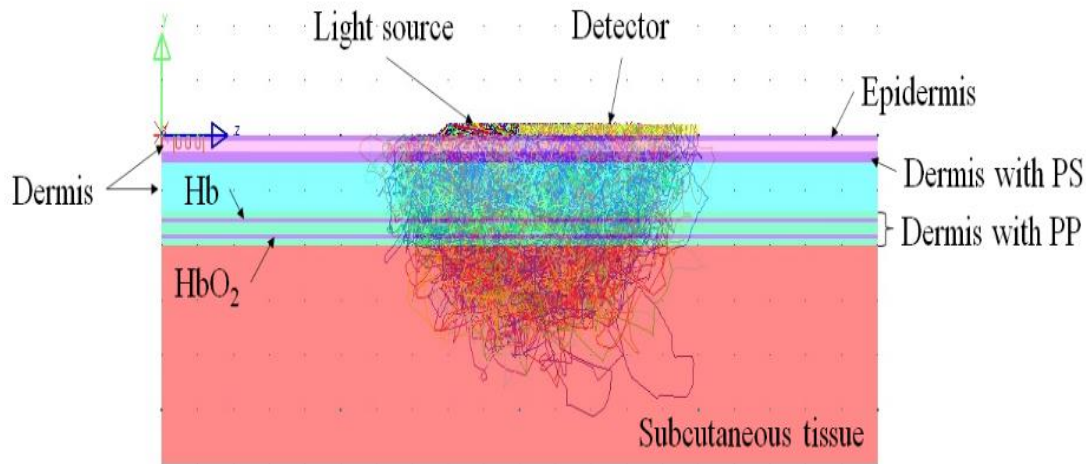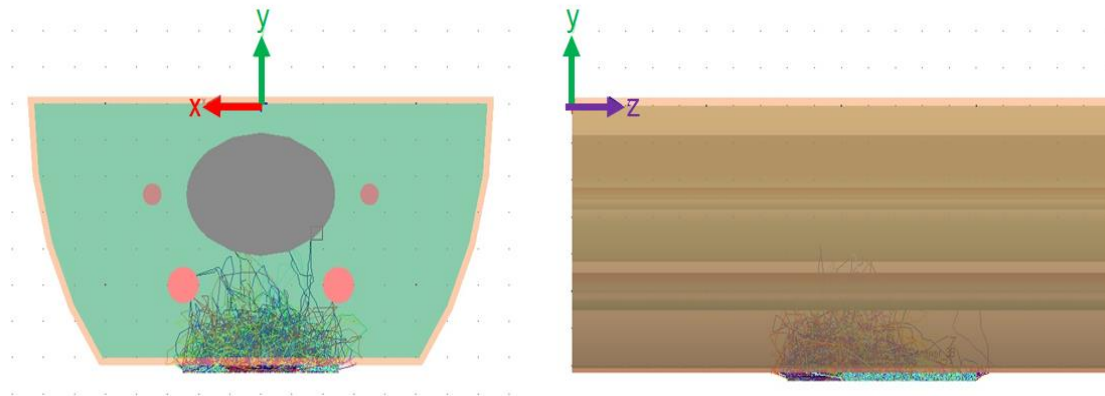

Figure 7. Filtered ray tracing distribution of the HbO_2 layer in the skin model

We fixed the distance between the source and detector for the fingertip model at 7 mm for transmission and 0 mm for reflection-based principles. Similar to the previous analysis, 10^5 numbers of rays were used for visualization purposes and 10^8 numbers of rays for data collection. For transmission-based structure, the distance was set to 7 mm by assuming the presence of a slight pressure applied onto the fingertip during the PPG measurement process, such as the clip-type PPG device. Based on Figure 8, the transmission-based principle shows a smaller number of rays arrived at the detector surface from the light source. One of the reasons is the long traveling path of the propagated light within the model. Another reason is the bone structure's high scattering effect, which hindered the light propagation.
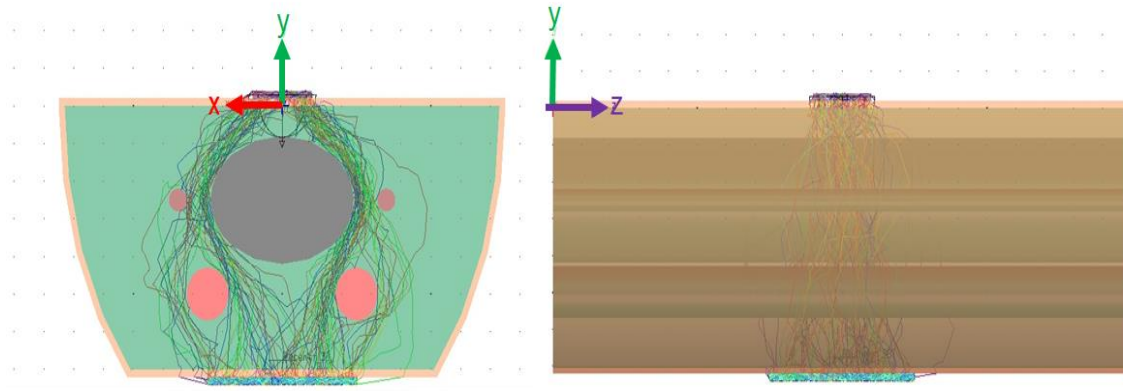
(a) Transmission-based with sectional view (left) and side view (right).

(b) Reflection-based with sectional view (left) and side view (right).

Figure 8.   Filtered ray tracing distribution of the HbO_2 from the artery in the fingertip structure

Pulsating condition

Figure 9 shows the signal intensity (both DC and AC components) from the skin model based on the number of photons detected on the surface of the detector at a different distance between the light source and the sensor. It shows a similar pattern as shown in Figure 2 previously, where the signal produced by the pulsating condition will increase as the HbO_2 volume increase. It also shows that the number of photons reduced as the distance increased in the diastole and systole conditions.

Figure 9.   Number of photons detected at the sensor surface for the diastole and systole conditions

We further analyzed the signals obtained from the simulation by converting them into electrical signals. We can estimate the photocurrent produced at the sensor based on the performance of the photodetector, which we developed previously and explained in detail elsewhere [5,7]. The current density was calculated based on the assumption that the photodetector's external quantum efficiency (EQE) is at 40%. The AC signals from the produced photocurrent at different distances between the source and detector are shown in Figure 10. As we increased the distance, the calculated photocurrent density significantly changed. At 0 mm to 2 mm distances between the source and detector, the estimated photocurrent was slightly reduced but still within a similar order of magnitude, around 10^{-10} A/mm^2. However, a significant photocurrent reduction was observed from 10^{-11} A/mm^2 to 10^{-12} A/mm^2 as we increased the distances from 3 mm to 5 mm. We suspected that it was due to the raised traveling path of the rays from the interest area as we increased the distance of the detector from the illuminated area. The scattering events in the turbid media are also an essential factor affecting the reflected light to the sensor.
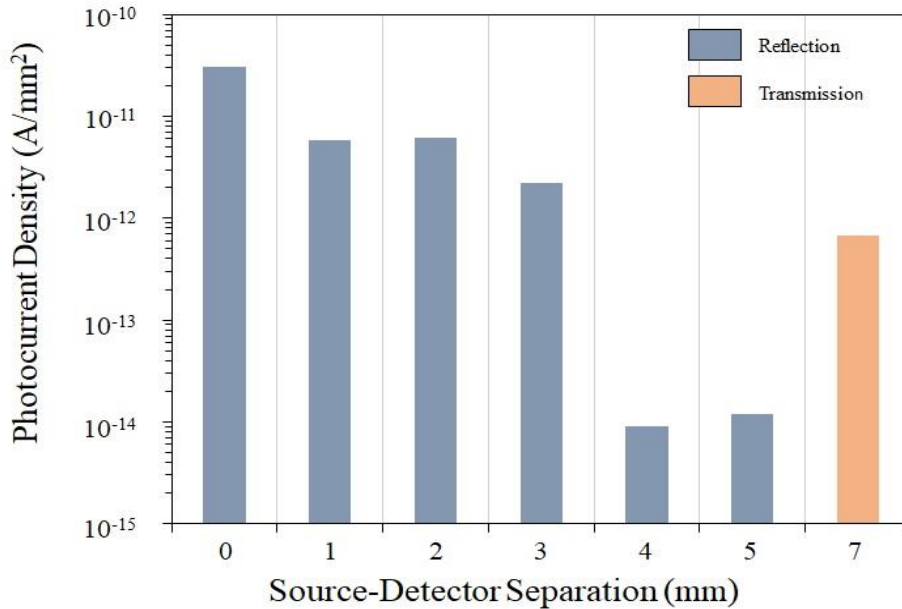
Figure 10. Estimated photocurrent density for AC component from the skin model at different source-detector separation

We also simulated both principles on the fingertip structure. The purpose was to observe the effect of the position or location between the source and detector. The photocurrent density for the reflection and transmission-based are shown in Figure 11. As expected, the closer distance between the source and detector has higher photocurrent density even in the fingertip model for the reflection-based, similar to the simulated skin model results. However, it is slightly different in the case of distance from 1 mm to 3 mm for both models. A linear decrease in photocurrent density was observed in the skin model, shown previously in Figure 10. Since we are assuming the homogeneous layer for each element for the skin model, thus the reduction shows linearity. In contrast, a slightly increased photocurrent density was observed at a 2 mm distance for the fingertip model. Even though the reason is still unknown, these photocurrent densities from 1 mm, 2 mm, and 3 mm distances were still within a similar order of magnitude at 10^{-12} A/mm^2. As we increased the distance further to 4 mm and 5 mm, a significant reduction of the photocurrent density was observed at 10^{-14} A/mm^2.

In the case of the transmission-based, the photocurrent density was two orders higher than the reflection-based at 4 mm and 5 mm distance with 10^{-12} A/mm^2. However, it is still lower than values for 0 mm to 3 mm distances. The position between the source and detector significantly impacts the sensing process. Here, the bone structure between them is one of the main reasons for the lower photocurrent density detected. The bone itself has higher opacity than other elements in the model. Thus, less light could penetrate the fingertip model and reach the sensor surface.

Figure 11. Estimated photocurrent density for AC component from the fingertip model at different source-detector separation for reflection and transmission-based

Conclusions

The ray-tracing MC simulation was performed to study the optical interactions in the turbid media for designing the PPG sensor device. In this study, we investigated the effect of the distance between the light source and detector, especially for the reflectance-based principle. We did the simulation using the skin and fingertip models at diastolic and systolic states, which correspond to the PPG waveform's cardiac cycle. We observed the ray-tracing behavior in the biological tissues for both principles, from the light source to the detector. The reflectance-based technique showed a higher photocurrent than the transmittance-based principle, up to a 3 mm separation distance between the light source and detector. The space more than 3 mm showed lower photocurrent detected than the transmittance-based at 7 mm. Therefore, we suggest that the optimal distance between the source and detector should be less than 3 mm for the reflectance-based PPG sensor device. Thus, we can enhance the PPG signal acquisition. The transmission-based simulation also showed that the position of the source and detector significantly impacted signal acquisition. In this principle, the bone structure is one of the high-opaque materials, which reduces the light penetration to the sensor on the other side. Thus, the reflectance-based has more significant advantage, especially for the wearable pulse oximetry device for a daily health monitoring system, due to its flexibility and quite convenient application on any body part. Plus, the separation distance between the light source and the detector for this principle can be tailored based on the microfabrication process for integrating these two devices.

References

[1] H. Lee, H. Ko, and J. Lee, "Reflectance pulse oximetry: Practical issues and limitations," *ICT Express*, vol. 2, no. 4, pp. 195–198, 2016, doi: 10.1016/j.icte.2016.10.004.

[2] E. D. Chan, M. M. Chan, and M. M. Chan, "Pulse oximetry: Understanding its basic principles facilitates appreciation of its limitations," *Respir. Med.*, vol. 107, no. 6, pp. 789–799, 2013, doi: 10.1016/j.rmed.2013.02.004.

[3] T. Tamura, Y. Maeda, M. Sekine, and M. Yoshida, "Wearable Photoplethysmographic Sensors-Past and Present," *electronics*, vol. 3, no. 2, pp. 282–302, 2014, doi: 10.3390/electronics3020282.

[4] A. Caizzone, A. Boukhayma, and C. Enz, "AC/DC Ratio Enhancement in Photoplethysmography Using a Pinned Photodiode," *IEEE Device Lett.*, vol. 40, no. 11, pp. 1828–1831, 2019, doi: 10.1109/LED.2019.2940063.

[5] A. Bilgaiyan, F. Elsamnah, H. Ishidai, C. -H. Shim, M. A. B. Misran, C. Adachi, and R. Hattori, "Enhancing Small-Molecule Organic Photodetector Performance for Reflectance-Mode Photoplethysmography Sensor Applications," *ACS Appl. Electron. Mater.*, vol. 2, no. 5, pp. 1280–1288, 2020, doi: 10.1021/acsaelm.0c00082.

[6] C. -Y. Huang, M. -C. Chan, C. -Y. Chen, and B. -S. Lin, "Novel Wearable and Wireless Ring-Type Pulse Oximeter with Multi-Detectors," *Sensors*, vol. 14, no. 9, pp. 17586-17599, 2014, doi: 10.3390/s140917586.

[7] F. Elsamnah, A. Bilgaiyan, M. Affiq, C. -H. Shim, H. Ishidai, and R. Hattori, "Reflectance-Based Organic Pulse Meter Sensor for Wireless Monitoring of Photoplethysmogram Signal," *Biosensors*, vol. 9, no. 3, pp. 87–100, 2019, doi: 10.3390/bios9030087.

[8] M. Hiraoka, M. Firbank, M. Essenpreis, M. Cope, S. R. Arridge, P. van der Zee, and D. T. Delpy, "A Monte Carlo investigation of optical pathlength in inhomogeneous tissue and its application to near-infrared spectroscopy," *Phys. Med. Biol.*, vol. 38, no. 12, pp. 1859–1876, 1876, doi: 10.1088/0031-9155/38/12/011.

[9] J. L. Reuss, and D. Siker, "The pulse in reflectance pulse oximetry: modeling and experimental studies," *J. Clin. Monit. Comput.*, vol. 18, no. 4, pp. 289–299, 2004, doi: 10.1007/s10877-005-2909-6.

[10] V. A. Peris, and S. Hu, "Validation of a Monte Carlo platform for the optical modelling of pulse oximetry," *J. Phys.: Conf. Ser.,* vol. 85, no. May 2007, pp. 012027, 2007, doi: 10.1088/1742-6596/85/1/012027.

[11] S. Chatterjee, and P. A. Kyriacou, "Monte Carlo Analyiss of Optical Interactions in Reflectance and Transmittance Finger Photoplethysmography," *sensors*, vol. 19, no. 4, pp. 789–807, 2019, doi: 10.3390/s19040789.

[12] K. -C. Huang, C. -L. Chang, H. -C. Chang, and C. -H. Chang, "The Image Analysis of Skin Tissue Irradiated with Difference Wavelengths of LED Sources," *2012 IEEE I2MTC – Int. Instrum. Meas. Technol. Conf. Proc.*, pp. 1246-1250, 2012, doi: 10.1109/I2MTC.2012.6229198.

[13] V. V. Tuchin, "Tissue Optics and Photonics: Biological Tissue Structures," *J. Biomed. Photonics eng.,* vol. 1, no. 1, pp. 3–21, 2015, doi: 10.18287/jbpe-2015-1-1-3.

[14]   V. V. Tuchin, "Tissue Optics and Photonics: Light-Tissue Interaction II," *J. Biomed. Photonics eng.,* vol. 2, no. 3, pp. 030201, 2016, doi: 10.18287/JBPE16.02.030201.

[15]   I. V. Meglinsky, and S. J. Matcher, "Modelling the sampling volume for skin blood oxygenation measurements," *Med. Biol. Eng. Comput.,* vol. 39, no. 1, pp. 44–50, 2001, doi: 10.1007/BF02345265.

[16]   I. V. Meglinsky, and S. J. Matcher, "Computer simulation of the skin reflectance spectra," *Comput. Methods Programs Biomed.,* vol. 70, no. 2, pp. 179–186, 2003, doi: 10.1016/S0169-2607(02)00099-8.

[17]   J. L. Latham, and S. N. Martin, "Infiltrative anesthesia in office practice," *Am. Fam. Physician,* vol. 89, no. 12, pp. 956–962, 2014, PMID: 25162162.

[18]   L. Jazayeri, J. Q. Klausner, and J. Chang, "Distal digital replantation," *Plast. Reconstr. Surg.,* vol. 132, no. 5, pp. 1207–1217, 2013, doi: 10.1097/PRS.0b013e3182a3c0e7.

[19]   C. Y. Chia, and T. Nassif, "Reintegration of distal digital amputation with composite graft and plasmatic diffusion expanded distally on the palmar dermal plane – a case report of a 2-year-old child and a literature review," *Rev. Bras. Cir. Plást.,* vol. 30, no. 3, pp. 495–500, 2015, doi: 10.5935/2177-1235.2015RBCP0185.

[20]   A. N. Bashkatov, E. A. Genina, and V. V. Tuchin, "Optical Properties of Skin and Subcutaneous Tissues," *J. Innov. Opt. Health Sci.,* vol. 4, no. 2, pp. 9–38, 2011, doi: 10.1142/S1793545811001319.

[21]   T. Lister, P. A. Wright, and P. H. Chappell, "Optical properties of human skin," *J. Biomed. Opt.,* vol. 17, no. 9, pp. 090901, 2012, doi: 10.1117/1.JBO.17.9.090901.

[22]   N. Bosschaart, G. J. Edelman, M. C. G. Aalders, T. G. van Leeuwen, and D. J. Faber, "A literature review and novel theoretical approach on the optical properties of whole blood," *Lasers Med. Sci.,* vol. 29, no. 2, pp. 453–479, 2014, doi: 10.1007/s10103-013-1446-7.